KONA Powder and Particle Journal

KONA Powder and Particle Journal No. 42 (2025) 156–169/https://doi.org/10.14356/kona.2025003 Review Paper

Synthesis of Functional Nanoparticles Using a Microreactor†

Satoshi Watanabe* and Minoru T. Miyahara#

Department of Chemical Engineering, Kyoto University, Japan

Fine particles are widely used as intermediate and final products in industrial processes. Because particle properties are directly linked to the function and quality of the products, synthesizing monodispersed particles is a key technology. A microreactor, which comprises microchannels typically narrower than 1 mm, is a promising reaction tool because it offers excellent mixing and heat transfer performance. We used a microreactor for the synthesis of single-component and composite nanoparticles. This review introduces our synthetic results for functional nanoparticles including nickel, platinum–cobalt alloys, gold and silver nanoshells, patchy particles, core–shell clusters, and metal–organic frameworks. The microreactor we used is of the central-collision type and exhibits a characteristic mixing time 100~1,000 times shorter than that of the conventional batch mixing. The excellent mixing ability of the microreactor enables the synthesis of monodisperse particles in size and shape as well as core–shell particles with uniform shell thickness through instantaneous nucleation. More importantly, the microreactor realizes syntheses, which are not possible with batch reactors, by trapping reaction intermediates in a sequential reaction process and by rapidly changing the reaction temperature. These results demonstrate great advantages of using the microreactor for nanoparticle synthesis.

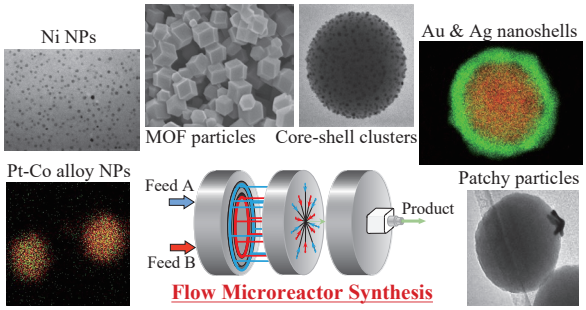

Keywords: microreactor, alloy nanoparticles, core–shell particles, metal–organic frameworks, nucleation, mixing time

1. Introduction

Fine particles are core materials in various industries, including chemistry, cosmetics, electronics, food, pharmaceuticals, photonics, and printing. Even if the final products are not in the particulate form, particles are contained in liquid and solid form products, including sunscreens, paint, and colored glasses, and they are involved in many products as intermediates in industrial processes. Notably, nanoparticles (NPs) play key roles in various applications, including electrode catalysts for fuel cells (Hou J. et al., 2020), conductive pastes (Abhinav K V. et al., 2015), bioimaging (Wolfbeis O.S., 2015), and sensing devices (Saha K. et al., 2012). In these applications, particle properties are directly linked to the function and quality of the products, and accordingly, the synthesis of monodispersed NPs in size and shape is a crucial issue.

Among various synthetic processes of NPs reported so far, liquid-phase synthesis using chemical reactions is promising in terms of versatility in reaction conditions and ease of process handling (Fiévet F. et al., 2018; Wang D. and Li Y., 2011; Xia Y. et al., 2009). A general strategy for synthesizing monodispersed particles is to shorten the nucleation period so that the particle growth period starts after the completion of nucleation. However, conventional batch-type synthesis often allows overlap between nucleation and growth periods because of its weak mixing intensity, which causes concentration distribution after mixing reaction solutions, resulting in the formation of particles with a wide size distribution. “Slowing reaction rates” is a possible solution because the effect of mixing becomes less significant, but typically leads to the formation of particles of submicrometer size or larger. In contrast, “quickening mixing rates” is a more direct and promising approach that is suitable for NP synthesis, which typically involves rapid reactions.

To achieve the latter approach, a microreactor is the first candidate because rapid mixing is a primary feature of microreactors (Yoshida J. et al., 2013). Microreactors comprise microchannels typically narrower than 1 mm, in which chemical reactions occur. Not only mixing ability but also heat transfer is excellent in microspaces, and accordingly exploiting these properties dramatically improves the precision and efficiency of chemical reactions (Mae K., 2007). Microreactors with different architectures have been successfully applied to the synthesis of various types of NPs, including gold using a chip-based interdiffusion microreactor (Wagner J. et al., 2004) and a chip-shaped three-layer assembly (Wagner J. and Köhler J.M., 2005), silver using a tubular (Lin X.Z. et al., 2004) and helical microreactors (Wu K.-J. et al., 2017), platinum using a droplet junction chip (Luty-Błocho M. et al., 2013)

† Received 5 July 2023; Accepted 28 September 2023
J-STAGE Advance published online 24 February 2024
* Corresponding author: Satoshi Watanabe;
Add: Katsura, Nishikyo, Kyoto 615-8510, Japan
E-mail: nabe@cheme.kyoto-u.ac.jp
TEL: +81-75-383-2682 FAX: +81-75-383-2652
Minoru T. Miyahara passed away on August 11, 2022.

and a spiral tubular microreactor (Suryawanshi P.L. et al., 2016), palladium using a Y-junction microreactor (Sharada S. et al., 2016) and a slit interdigital microstructured mixer (Gioria E. et al., 2019), nickel using a T-shaped microreactor (Xu L. et al., 2015), and silica in a slit interdigital microstructured mixer (Gutierrez L. et al., 2011). Not only single-component NPs and composite particles have been synthesized, including palladium@platinum core–shell nanoparticles using T-mixers (Hashiguchi Y. et al., 2021), gold nanoshells in microfluidic slug flow (Duraiswamy S. and Khan S.A., 2010), and patchy particles using a T-mixer (Meincke T. et al., 2017; Völkl A. and Klupp Taylor R.N., 2022). Microreactors combined with acoustic waves to enhance mixing intensity, which are so-called acoustic microreactors, have also been demonstrated to synthesize various types of NPs (Chen Z. et al., 2022). These synthetic results demonstrate the advantages of applying microreactors to NP synthesis.

Focusing especially on the excellent mixing ability of microreactors, we have been working on the synthesis of functional NPs such as nickel (Ni) and bimetallic alloy (Watanabe S. et al., 2021), nanoporous metal–organic frameworks (MOFs) (Fujiwara A. et al., 2021; Watanabe S. et al., 2017b), gold and silver nanoshells (Maw S.S. et al., 2019; Watanabe S. et al., 2015), and patchy particles (Watanabe S. et al., 2016). Our concept is to achieve highly supersaturated conditions by quickly mixing reaction solutions, thereby enabling instantaneous nucleation and subsequent growth. In this review article, we introduce our synthetic results using a microreactor.

2. Central-collision-type microreactor

The microreactor we used is a central-collision-type reactor (Nagasawa H. et al., 2005), which comprises three plates (inlet, mixing, and outlet plates), as illustrated in **Fig. 1**. Each of the two inlet fluids is divided into seven streams on the inlet plate (**Fig. 1(B)**), and the fourteen streams (seven from inlet A indicated by black circles and the other seven from inlet B indicated by black squares as illustrated in **Fig. 1(C)**) collide with each other into a single stream at the center of the mixing plate and then outflow from the outlet. We used the microreactor with fourteen streams because the mixing intensity was confirmed to increase with the number of streams (Nagasawa H. et al., 2005) and fourteen streams were almost the highest possible number in terms of channel geometry. The intensive collision breaks the fluids into small segments, thereby shortening the diffusion distance to achieve quick mixing.

We evaluated the mixing ability of the microreactor using a chemical test reaction (Watanabe S. et al., 2017a). We adopted the Villermaux–Dushman (VD) method (Ehrfeld W. et al., 1999; Fournier M.C. et al., 1996), which comprises parallel competing neutralization and redox reactions. Because the neutralization reaction is much faster than the redox reaction, only the neutralization reaction would proceed under ideal mixing conditions. However, in the case of poor mixing, the mixed fluid is segregated, and accordingly, the redox reaction proceeds. Thus, the amount of the product from the redox reaction is a measure of the mixing intensity (smaller production indicates better mixing). We obtained the mixing time from the VD experiments following the procedure reported by Commenge et al. (Commenge J.-M. and Falk L., 2011). **Fig. 2** shows the relationship between the mixing time t_m and the flow rate. The increase in the flow rate shortens the mixing time of the microreactor, and a flow rate of 10 mL/min attains the shortest mixing time of 0.3 ms, which indicates that complete mixing is achieved in 0.3 ms. For comparison purposes, **Fig. 2** also shows a series of mixing times of a Y-shaped mixer with an inner diameter of 1.5 mm. At the

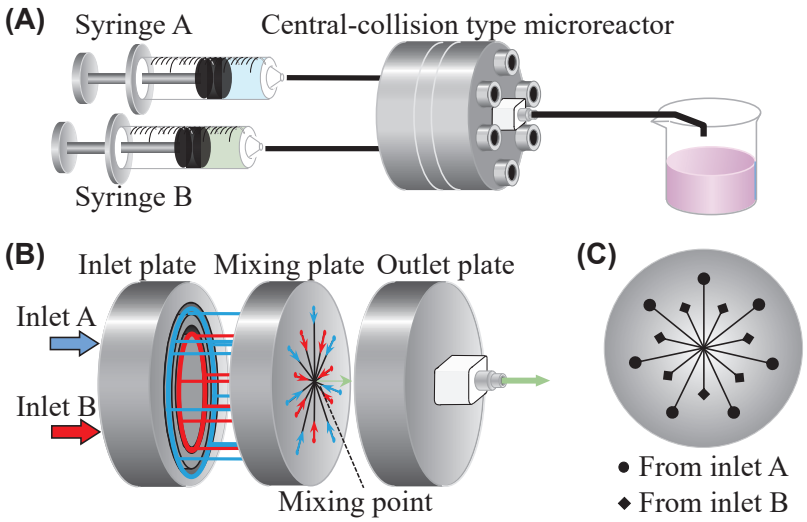

Fig. 1 Schematic illustrations of **(A)** experimental setup for nanoparticle synthesis, **(B)** central-collision-type microreactor (disassembly image), and **(C)** mixing plate. Adapted with permission from Ref. (Watanabe S. et al., 2017a). Copyright: (2017) Elsevier B.V.

same flow rates, the mixing time of the microreactor is 100~1,000 times shorter than that of the Y-shaped mixer, clearly demonstrating the advantage of the microreactor. Comparison of the microreactor with the Y-shaped mixer and batch-type reactor under the same Reynolds numbers from 300 to 1200 also confirmed the superiority of the microreactor in terms of mixing intensity. A short mixing time leads to a uniform reaction field with the desired concentration condition, thereby enabling the formation of monodisperse particles.

3. Synthesis of metallic nanoparticles

Metallic particles exhibit excellent chemical and physical properties, and are thus promising in various applications, including catalysts, electronics, photonics, sensing, and imaging (Xia Y. et al., 2009). Downsizing them to the nanoscale is crucial to fully exploit their properties. Here we focus on Ni, and Ni NPs with average diameters of 3–10 nm have been synthesized by several techniques, including a water-in-oil microemulsion technique (Chen D.-H. and Wu S.-H., 2000; Wu X. et al., 2012), an organometallic approach (Domínguez-Crespo M.A. et al., 2009; Ely T.O. et al., 1999), and a polyol process (Couto G.G. et al., 2007; Eluri R. and Paul B., 2012; Wu S.-H. and Chen D.-H., 2003). However, these techniques rely on organic solvents and involve heating during the synthesis, which can be a problem in terms of environmental protection and energy consumption. Although aqueous syntheses have been reported (Chen D.-H. and Hsieh C.-H., 2002; Jiang Z. et al., 2013), the resultant size of Ni particles was larger (>10 nm) with wider size distributions than those synthesized using organic solvents. Why is it so difficult to synthesize monodisperse Ni NPs in aqueous systems? This is because the reduction reaction of Ni ions does not uniformly proceed due to insufficient mixing, and if this is the case, the central-collision-type microreactor is a suitable reactor to overcome this difficulty.

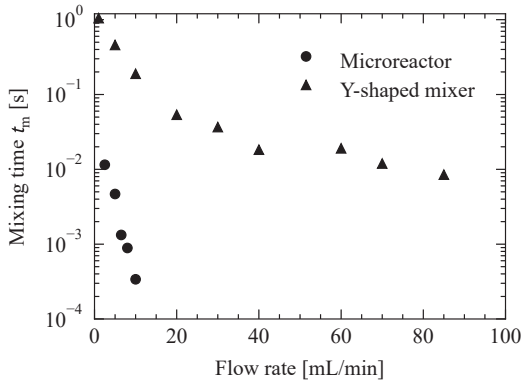

Fig. 2 Dependence of the characteristic mixing time (t_m) estimated from the VD experiments on the flow rate for different mixing procedures of the microreactor and Y-shaped mixer. Adapted with permission from Ref. (Watanabe S. et al., 2017a). Copyright: (2017) Elsevier B.V.

Fig. 3 shows the experimental setup for Ni NPs synthesis, in which two microreactors are sequentially connected through a tube with varying lengths of 1, 3, 20, and 40 cm (Watanabe S. et al., 2021). Varying the tube length corresponded to the change in residence times between the two microreactors (0.053, 0.16, 1.1, and 2.1 s). We first mixed aqueous solutions of $NiCl_2$ and a surfactant (cetyltrimethylammonium bromide; CTAB). We used CTAB because it has been reported to serve as an effective capping agent suitable for the Ni NP synthesis (Wu S.-H. and Chen D.-H., 2004). The premixed solution was mixed with a hydrazine (N_2H_4) aqueous solution in microreactor A, and the mixed solution from the outlet, which was directly injected into microreactor B, was mixed with a sodium hydroxide (NaOH) solution. The flow rate was set to 10 mL/min for each syringe using syringe pumps, and the synthesis was conducted at room temperature. In this sequential flow process, the following reaction scheme is assumed (Park J.W. et al., 2006). The reaction in microreactor A produces nickel–hydrazine complexes.

$$Ni^{2+} + xN_2H_4 \rightarrow \left[Ni\left(N_2H_4\right)_x\right]^{2+}, x = 1,2,3 \quad (1)$$

Subsequent mixing with NaOH in microreactor B induces a ligand exchange reaction to yield nickel hydroxide ($Ni(OH)_2$) and N_2H_4.

$$\left[Ni\left(N_2H_4\right)_x\right]^{2+} + 2OH^- \rightarrow Ni\left(OH\right)_2 + xN_2H_4 \quad (2)$$

$Ni(OH)_2$ was then reduced to zero-valent Ni by freed N_2H_4, followed by nucleation and growth to produce Ni

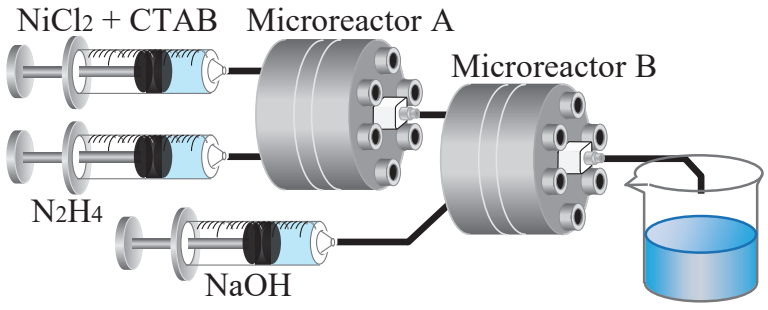

Fig. 3 Schematic of the sequential flow process for the synthesis of Ni NPs. Reprinted from Ref. (Watanabe S. et al., 2021) under the terms of the CC-BY 4.0 license. Copyright: (2021) The Authors, published by Frontiers.

NPs.

A typical synthetic result is presented in **Fig. 4**, where the residence time between microreactors A and B was set to 0.053 s. NPs with a sharp size distribution (3.8 ± 0.6 nm) were successfully formed, as confirmed by transmission electron microscopy (TEM) images and particle size distributions (**Figs. 4(A) and 4(B)**). X-ray photoelectron spectroscopy (XPS) and powder X-ray diffraction (XRD) measurements demonstrated the formation of Ni NPs with face-centered cubic (fcc) crystal structures (**Figs. 4(C) and 4(D)**). The synthesized Ni NPs were comparable to those synthesized using organic solvents in terms of average particle size and size distribution, demonstrating the excellent performance of the microreactor that enables aqueous and room-temperature synthesis of Ni NPs. Note that the use of a Y-shaped mixer with a weaker mixing intensity in place of either microreactor A or B did not produce monodisperse Ni NPs, further demonstrating the importance of the instantaneous and homogeneous mixing provided by the microreactor for the synthesis of monodisperse NPs.

In this flow sequential process, the residence time between microreactors A and B was found to have a critical effect on the size distribution; a longer residence time resulted in a wider distribution. This is closely related to the formation of nickel–hydrazine complexes. Ni ions are reported to react with N_2H_4 molecules to form stable three-coordinate complex structures $[Ni(N_2H_4)_3]^{2+}$, by way of intermediate species with one- and two-coordinate structures $[Ni(N_2H_4)]^{2+}$ and $[Ni(N_2H_4)_2]^{2+}$ (Gilbert E.C. and Evans W.H., 1951; Li Y.D. et al., 1999). A residence time of more than 2 s is assumed to be sufficiently long to allow the formation of stable three-coordinate complex structures before mixing with NaOH. In this case, the ligand exchange reaction would be slow, possibly because of the high activation energy required to replace N_2H_4 molecules with OH^- ions (**Eqn. (2)**), which leads to a slow reduction and consequently results in a wide size distribution. In contrast, under residence times shorter than ca. 1 s, less stable intermediate species react with NaOH to quickly free N_2H_4 molecules through the ligand exchange reaction, thereby leading to a quick reduction of Ni ions. In this manner, for the formation of monodisperse Ni NPs, it is necessary to trap less stable intermediate complex structures so that they react with NaOH at microreactor B. To satisfy this requirement, precise control of the residence time, on the order of milliseconds, is critical, which is enabled by the excellent mixing performance of the microreactor.

The synthesis of bimetallic alloy NPs is also possible using a central-collision-type microreactor. We synthesized platinum (Pt)–cobalt (Co) alloy NPs by the simultaneous reduction of Pt and Co ions. We mixed a premixed aqueous solution of Pt and Co ions and polyvinylpyrrolidone (PVP, molecular weight of 1,300,000) with an aqueous solution of a strong reducing agent, $NaBH_4$, in the microreactor (**Fig. 1(A)**). We opted for PVP for two reasons: firstly, it is

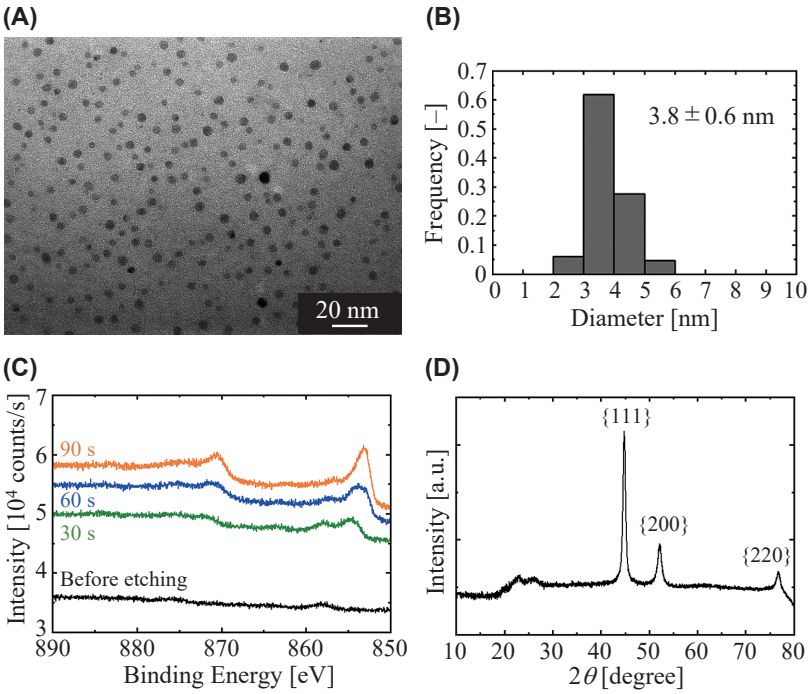

Fig. 4 Synthetic result of Ni NPs with a residence time of 0.053 s. **(A)** TEM image, **(B)** particle size distribution, **(C)** XPS result, and **(D)** XRD pattern. In the XPS result, the peaks at 870 and 853 eV were attributed to Ni $2p_{1/2}$ and Ni $2p_{3/2}$, respectively, which appeared after Ar ion etching, possibly because the etching removed CTAB molecules surrounding the resultant particle surfaces. Reprinted from Ref. (Watanabe S. et al., 2021) under the terms of the CC-BY 4.0 license. Copyright: (2021) The Authors, published by Frontiers.

widely used as a stabilizer for various metallic NPs, and secondly, being a nonionic polymer, it is suitable for investigating the effects of different metal precursors—details of which are discussed later. This choice prevents the dissolution of different ions from stabilizers. **Fig. 5** presents TEM images, particle size distributions, and scanning TEM (STEM) and energy-dispersive X-ray (EDX) mapping images of the resultant particles synthesized using the microreactor (**Fig. 5(A)**) and a batch reactor (**Fig. 5(B)**) for comparison, in which K_2PtCl_4 and $CoCl_2$ were used as precursors. The microreactor produced NPs with a monomodal distribution, which is in contrast to batch reactor synthesis, which results in a wide size distribution with a rather bimodal shape. As shown in the STEM and EDX mapping images, in the case of the microreactor, Pt and Co elements were uniformly mixed in single particles to form solid solutions, whereas the batch reactor yielded segregated structures composed of smaller (Co) and larger (Pt) NPs.

The results shown in **Fig. 5** again demonstrate the importance of the mixing process in NP synthesis because the mixing procedure (microreactor vs. batch reactor) is the only difference in the synthetic processes. The formation of segregated particles from the batch reactor can be explained as follows: because of the weak mixing ability of the batch reactor, a reaction solution immediately after mixing two solutions is non-uniform and has domains of the original solutions with different sizes. In this situation, reducing agents can be locally deficient relative to metal ions, and accordingly, Pt ions are preferentially reduced because of their lower ionization tendency than that of Co ions to promote the nucleation of Pt and subsequent growth. This results in the formation of larger Pt NPs. Consequently, the resultant particles exhibit segregated bimodal structures composed of larger Pt and smaller Co NPs. In contrast, complete mixing is achieved much faster in the microreactor, and the reaction solution is more uniform. In this homogeneously mixed solution, the reduction reaction of both Pt and Co ions simultaneously proceeds to produce Pt–Co solid solution alloys.

For the synthesis of Pt–Co solid solution alloy NPs, the choice of precursors was critical (**Fig. 6**). For a fixed Co precursor of $CoCl_2$, the resultant particles were Pt–Co solid solution alloys when K_2PtCl_4 was used as a Pt precursor (**Fig. 6(A)**), whereas the use of H_2PtCl_6 resulted in the formation of smaller NPs mainly composed of Pt as well as larger Pt–Co alloy NPs (**Fig. 6(C)**). We also used K_2PtCl_6 and confirmed a similar result to that of H_2PtCl_6. A different Co precursor ($Co(NO_3)_2$) yielded similar results to those of $CoCl_2$ (**Figs. 6(B) and 6(D)**). These results demonstrate that the valence number of Pt ions is more critical than the type of Co precursors and counter cations in Pt precursors; for synthesizing monodisperse Pt–Co alloy NPs, the use of $PtCl_4^{2-}$ ions is more desirable than $PtCl_6^{2-}$ ions. $PtCl_4^{2-}$ ions

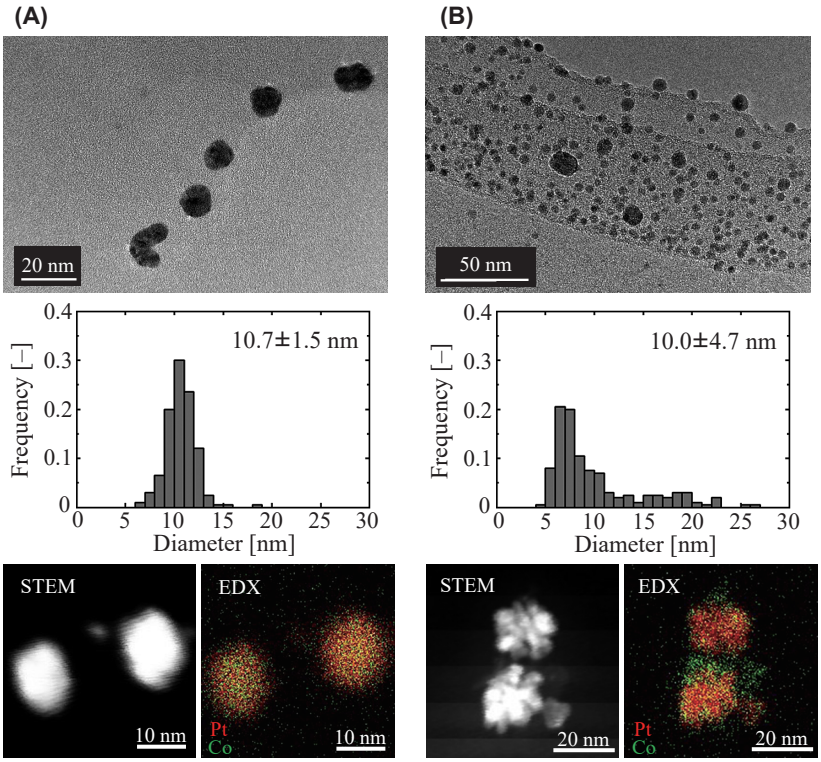

Fig. 5 TEM image, particle size distribution, and STEM and EDX mapping images of Pt and Co bimetallic particles synthesized by **(A)** microreactor and **(B)** batch reactor. Reprinted from Ref. (Watanabe S. et al., 2021) under the terms of the CC-BY 4.0 license. Copyright: (2021) The Authors, published by Frontiers.

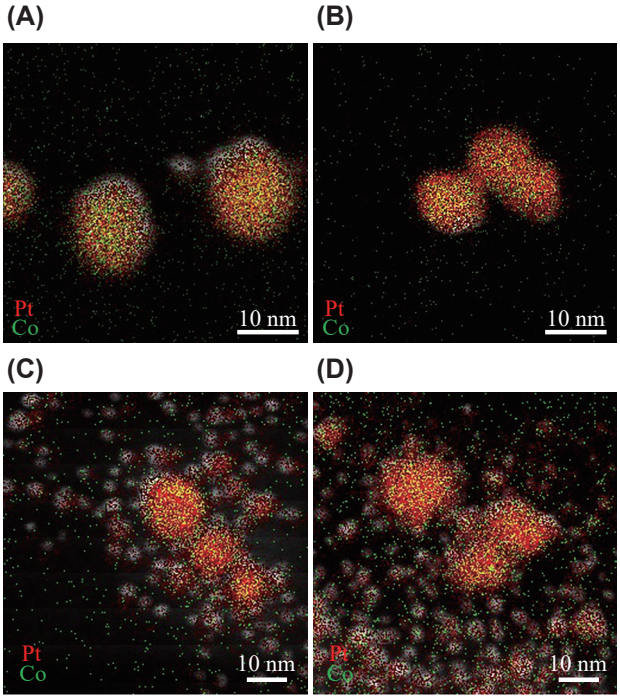

Fig. 6 EDX mapping images of Pt and Co bimetallic particles synthesized from different combinations of precursors of **(A)** K_2PtCl_4 and $CoCl_2$, **(B)** K_2PtCl_4 and $Co(NO_3)_2$, **(C)** H_2PtCl_6 and $CoCl_2$, and **(D)** H_2PtCl_6 and $Co(NO_3)_2$. Reprinted from Ref. (Watanabe S. et al., 2021) under the terms of the CC-BY 4.0 license. Copyright: (2021) The Authors, published by Frontiers.

are directly reduced to zero-valent Pt, while $PtCl_6^{2-}$ ions follow a two-step sequential route by way of $PtCl_4^{2-}$ ions. Because the standard reduction potentials of $PtCl_6^{2-}$/$PtCl_4^{2-}$ and $PtCl_4^{2-}$/Pt are similar (Jiang B. et al., 2015), the reduction reaction of $PtCl_6^{2-}$ ions would be slower than that of $PtCl_4^{2-}$ to have a rate difference in the reduction reaction of Co ions. Because of the difference in the reduction rate, $PtCl_6^{2-}$ is later reduced to produce smaller NPs with a main component of Pt. Therefore, matching the reduction rates of constituent metal ions is another key factor for synthesizing solid solution alloy NPs.

4. Synthesis of metallic shells and patches

Core–shell-type particles with metallic shells and dielectric cores, or so-called metallic nanoshells, are quite promising for optical and biomedical applications because of their tunable surface plasmon resonances (Yang W. et al., 2019). Not only metallic nanoshells but also core–shell clusters (CSC; core particles uniformly covered with nanoparticles) and patchy particles (core particles partially covered with shell portion) exhibit attractive optical properties due to discreteness and/or anisotropy in the particle structure (Han J.H. et al., 2022; Mühlig S. et al., 2011). What is intriguing about these composite particles is that they not only possess multiple different properties, which is impossible with single-component particles, but also demonstrate peculiar characteristics due to synergetic effects, interfacial properties, and morphologies of core and shell materials. However, because of the complexity of their structures, the synthesis of these structured particles is generally not straightforward, and typically requires multiple steps and/or templates. In core–shell-type particle synthesis, controlling reactions on core particle surfaces is a major difficulty. It is generally challenging to promote reactions selectively at interfaces because reactions in the bulk phase can proceed in parallel, especially when reactions are quick.

Here, we take gold nanoshells as an example. A typical synthetic method is seed-mediated growth, which comprises three steps: surface modification of core silica particles, gold NP decoration of the modified silica surface as "seeds" to form CSCs, and growth of gold NP seeds into a shell by the reduction of gold ions (Oldenburg S.J. et al., 1998). Although this method allows good control in the shell thickness, it takes a long time, often on the order of days, to complete the preparation process. The bottleneck step is the CSC formation process, in which gold NPs are separately prepared by the reduction of gold ions, aged for a certain period of several days, and then mixed with a suspension of surface-modified silica particles to proceed with the adsorption of gold NPs on the modified silica surface, followed by the separation of unattached gold NPs (Rasch M.R. et al., 2009). Most of the syntheses of gold nanoshells are conducted in batch-type processes, and the intrinsic weak mixing ability of batch reactors is one of the reasons for the requirement of the multistep time-consuming procedure in the CSC formation process. This leads to the idea of using a microreactor to simplify and intensify the CSC formation process.

Our concept to achieve a one-step process for CSC formation was to simply use the principle that, under an ideally uniform reaction field, heterogeneous nucleation at interfaces is energetically more favored than homogeneous nucleation in the bulk phase. Following this concept, we mixed a premixed aqueous suspension of surface-modified silica particles and $HAuCl_4$ with an aqueous solution of $NaBH_4$ in a central-collision-type microreactor (**Fig. 1(A)**) (Watanabe S. et al., 2015). The surface modification of silica particles was conducted by using 3-aminopropyl trimethoxysilane to positively charge the particle surface. **Figs. 7(A) and 7(B)** present typical TEM images of the resultant particles, in which the core silica particles are uniformly decorated with monodisperse gold NPs. In our TEM measurements, we observed no unattached free gold NPs, indicating the preferential formation of gold NPs on the surface of core silica particles. In contrast, the use of a batch reactor and Y-shaped mixer (inner diameter of 1.5 mm) instead of the microreactor resulted in non-uniform deposition of gold NPs with wide size distributions, as shown in **Figs. 7(C) and 7(D)**. Another feature of **Figs. 7(C) and 7(D)** is that the gold NP coverages of

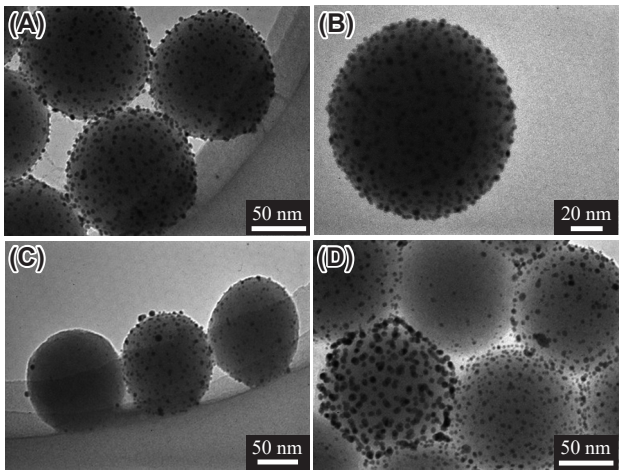

Fig. 7 Representative TEM images of CSCs prepared **(A,B)** with the microreactor, **(C)** with a batch reactor, and **(D)** with a Y-shaped mixer. Adapted with permission from Ref. (Watanabe S. et al., 2015). Copyright: (2015) Wiley.

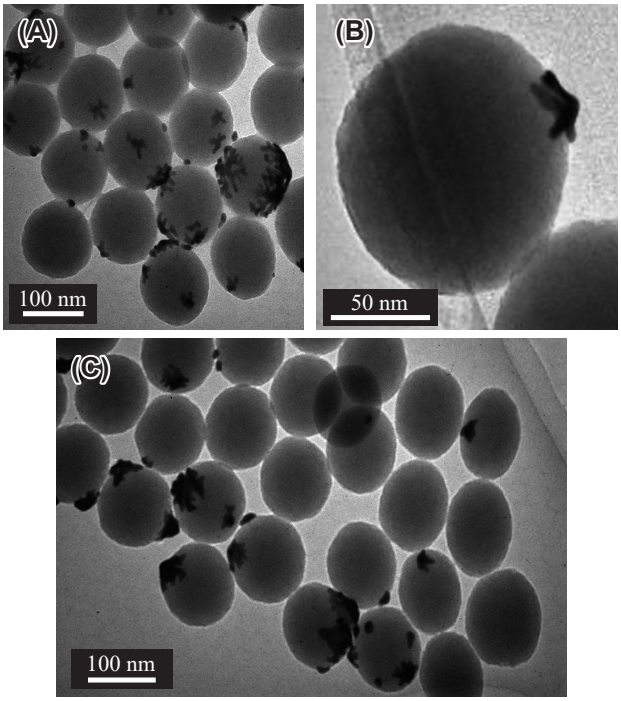

Fig. 8 Representative TEM images of patchy particles prepared **(A,B)** with the microreactor and **(C)** with a batch reactor. Adapted with permission from Ref. (Watanabe S. et al., 2016). Copyright: (2016) Elsevier B.V.

individual resultant CSCs are remarkably different between a state almost devoid of NPs and that with full decoration. Therefore, gold NP seeding through the in situ reduction of gold ions requires intensive mixing provided by the microreactor.

The in situ reduction of gold ions described above produced core silica particles uniformly decorated with gold NPs, which is possibly attributable to the use of a strong reducing agent, $NaBH_4$, which induced a rapid increase in the degree of supersaturation to produce many small nuclei. Based on this discussion, the use of a weaker reducing agent would lead to the formation of patchy particles. We accordingly used ascorbic acid as a reducing agent instead of $NaBH_4$, and as expected, we successfully obtained patchy particles (**Fig. 8(A)**) (Watanabe S. et al., 2016). Core particles are partially covered with gold patches with a dendritic shape (**Fig. 8(B)**), which is quite a contrast to the CSCs obtained using $NaBH_4$. Meanwhile, the batch-type reactor produced particles with a larger variation in the number of patches than the microreactor, as shown in **Fig. 8(C)**. These results demonstrate that even though a weaker reductant was used, the reduction reaction remained so rapid that intensive mixing by the microreactor was still necessary to obtain uniform patchy particles.

Based on these results, we propose possible formation mechanisms of CSCs and patchy particles, schematic representations of which are shown in **Fig. 9**. Before starting the reduction reaction in both cases, it is reasonable to assume that negatively charged gold complex ions form electric double layers by crowding around surface-modified silica particles with positive charges, as depicted in **Fig. 9(A)-(i)**. For CSC formation, upon mixing with a strong reducing agent, $NaBH_4$, the reduction of gold ions quickly proceeds to increase the degree of supersaturation of the reduced gold atoms. Due to the formation of electric double layers, the degree of supersaturation is higher in the vicinity of the particle surface than that of the bulk solution, thus leading to increased nucleation at the interface. Because gold NPs are negatively charged, they are stabilized on the surface of the surface-modified silica particles, which facilitates heterogeneous nucleation (**Fig. 9(A)-(ii)**). The nuclei formed on the silica particle surface grow larger through the diffusion of reduced gold atoms remaining in the vicinity of the core silica particles to complete the formation of CSCs (**Fig. 9(A)-(iii)**). In the case of ascorbic acid with a weak reducing ability, the degree of supersaturation is lower than that of $NaBH_4$; accordingly, a much fewer number of nuclei are formed on the core particle surface (**Fig. 9(B)-(i)**). In the subsequent growth process, the surface diffusion of reduced gold atoms along the core particle surface is dominant over that from the bulk phase because of the higher concentration of gold ions forming electric double layers (**Fig. 9(B)-(ii)**). Because the surface reaction of the patches is assumed to be quick, the growth reaction proceeds under diffusion-limited conditions. In this case, the protruding portions of patches preferentially grow, resulting in dendritic structures (**Fig. 9(B)-(iii)**).

According to this mechanism, not only the supply rate of gold, which is affected by the gold ion concentration and the reducing ability, but also the zeta potential of core particles is a critical factor for the resultant structure because the zeta potential dominantly determines the affinity with negatively charged gold ion complexes. To change the zeta

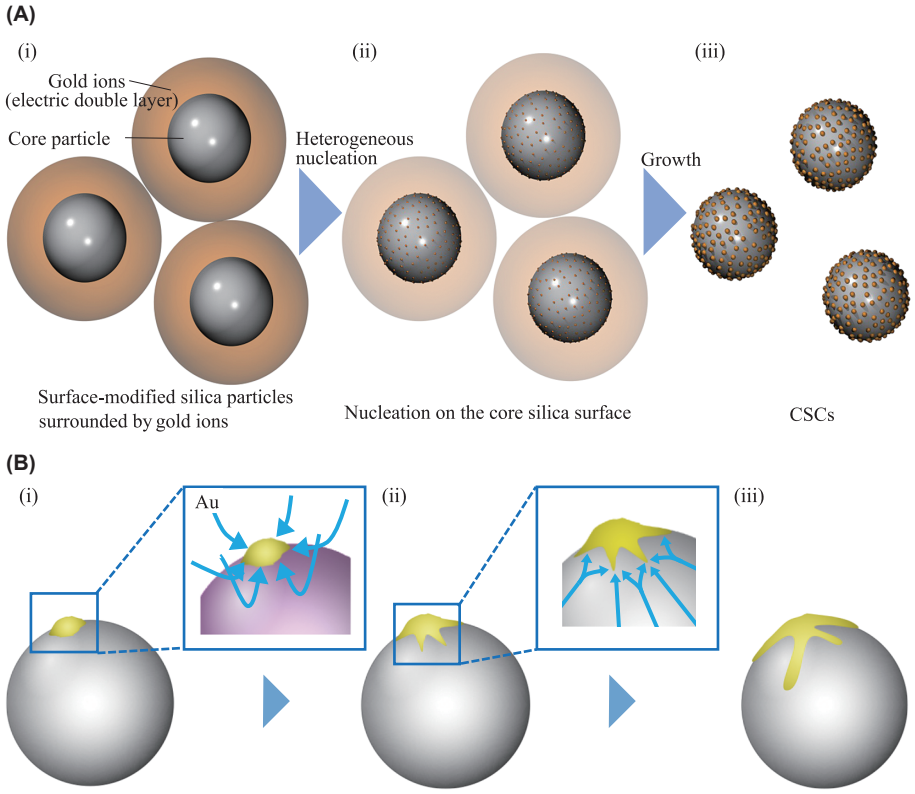

Fig. 9 Schematic of possible formation mechanisms of **(A)** CSCs and **(B)** patchy particles through the in situ reduction of gold ions. Adapted with permission from Refs. (Watanabe S. et al., 2015) and (Watanabe S. et al., 2016) for **(A)** and **(B)**, respectively. Copyrights: (2015) Wiley and (2016) Elsevier B.V.

potential and the supply rate, we used trisodium citrate, which has a much weaker reducing ability. The zeta potential of core silica particles decreased under higher pH conditions of a trisodium citrate solution. Under an increased temperature of 95 °C, we obtained "snowman-like" particles in which a gold NP with a diameter of approximately 30 nm was deposited on a core silica particle (Watanabe S. et al., 2016). The formation of these particles occurs because the use of a far weaker reducing agent highly suppressed nucleation and because the lowered zeta potential allowed diffusion from the bulk phase to form spherical patches. In this manner, the coating structure of the core silica particles can be manipulated by the supply rate of gold and the interaction between the core particles and gold ions.

Growing gold NP seeds from a CSC into a continuous shell leads to the formation of gold nanoshells. In the experiment, we mixed a premixed aqueous suspension of CSCs and gold ions with an aqueous solution of a reducing agent in a central-collision-type microreactor (**Fig. 1(A)**). Gold ions were obtained by preaging a $HAuCl_4$ solution with K_2CO_3, which is referred to as K-gold. In the shell growth process, the use of $NaBH_4$ as a reducing agent did not produce complete shells; seed gold NPs grew larger, although gold NPs newly formed in the bulk solution phase before completing shell formation (Watanabe S. et al., 2013). This is possibly because the energy barrier to self-nucleation in the bulk phase can be easily surmounted by the strong reducing ability of $NaBH_4$. We accordingly used a weaker reducing agent, ascorbic acid, and successfully synthesized complete gold nanoshells without self-nucleation in the bulk phase (**Fig. 10(A)**) (Watanabe S. et al., 2015). The shell thickness varied from 17 nm to 50 nm by changing the concentration of K-gold. In contrast, the use of a Y-shaped mixer (inner diameter of 1.5 mm) instead of the microreactor resulted in a mixture composed of unreacted particles (CSCs; the upper right particle in **Fig. 10(B)**), particles in the process of growing (the lower left particle in **Fig. 10(B)**), and gold nanoshells (the centered particle in **Fig. 10(B)**). The batch reaction also failed.

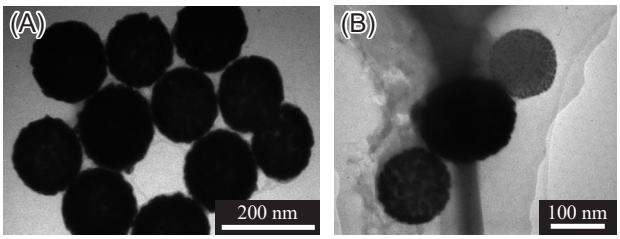

Fig. 10 Representative TEM images of the resultant particles after the shell growth reaction using **(A)** the microreactor and **(B)** a Y-shaped mixer. Adapted with permission from Ref. (Watanabe S. et al., 2015). Copyright: (2015) Wiley.

These results are similar to the case of the formation of CSCs and patchy particles, thereby demonstrating that strong mixing by the microreactor is necessary for the synthesis of uniform gold nanoshells. By using $AgNO_3$ mixed with ammonia instead of K-gold and formaldehyde as a reducing agent, silver nanoshells can be synthesized (**Fig. 11**) (Maw S.S. et al., 2019), demonstrating the versatility of the synthetic process using a microreactor.

Taking advantage of the flow processes, we combined the synthetic processes for CSCs and gold nanoshells into a sequential process (**Fig. 12(A)**). A premixed suspension of surface-modified silica particles and $HAuCl_4$ was mixed with $NaBH_4$ in the first microreactor to produce CSCs, followed by mixing with K-gold in a Y-shaped mixer. The mixed suspension from the Y-shaped mixer was directly injected into the second microreactor to react with ascorbic acid to yield gold nanoshells. Residence times between the first microreactor and the Y-shaped mixer and between the Y-shaped mixer and the second microreactor were set to be 2 s and 1 s, respectively, which are considerably longer than the mixing times (~0.3 ms for the microreactor and ~50 ms for the Y-shaped mixer). This attempt was successful because uniform gold nanoshells were synthesized without the formation of gold NPs in the bulk solution phase, as shown in **Figs. 12(B)** and **12(C)** (Watanabe S. et al., 2015). Our sequential flow process not only enables a high throughput of 60 mL/min compared with typical microfluidic systems but also reduces tedious efforts such as post-synthetic washing steps to remove free unattached gold NPs. For the silver nanoshell synthesis, a sequential flow process similar to the case of the gold nanoshells was attempted but resulted in the formation of free silver NPs, possibly because silver ions were reduced by the remaining $NaBH_4$ after the CSC formation reaction. To deactivate $NaBH_4$, we found that a longer residence time of ~30 min between the CSC formation and the shell growth reactions was necessary, and with that setting of a long residence time, the flow sequential synthesis of silver nanoshells is in principle possible. This type of flow sequential process enables the facile and scalable synthesis of metallic nanoshells and is accordingly promising for industrial applications in various fields.

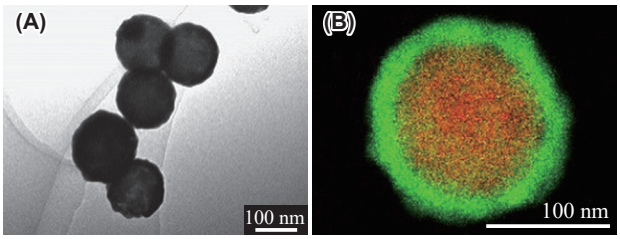

Fig. 11 **(A)** TEM and **(B)** STEM-EDX mapping (Si: red, Ag: green) images of the resultant silver nanoshells synthesized using the microreactor. Adapted with permission from Ref. (Maw S.S. et al., 2019). Copyright: (2019) Elsevier B.V.

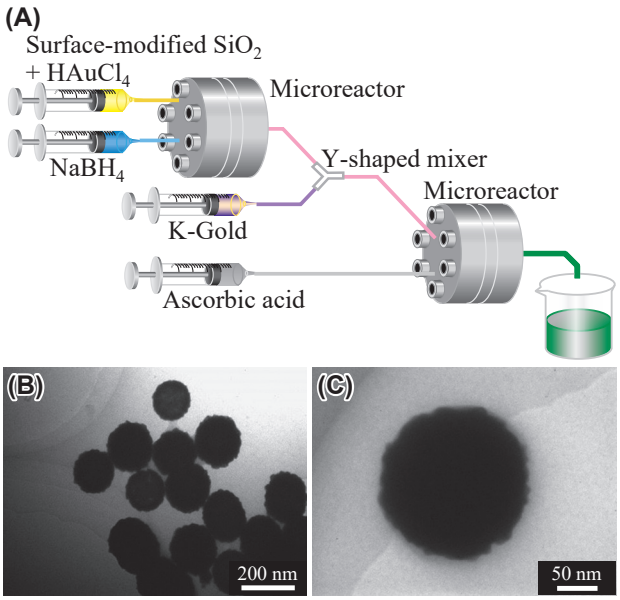

Fig. 12 **(A)** Schematic of the experimental setup for the sequential flow synthesis of gold nanoshells from surface-modified silica particles. **(B,C)** TEM images of the resultant gold nanoshells. Adapted with permission from Ref. (Watanabe S. et al., 2015). Copyright: (2015) Wiley.

5. Synthesis of nanoporous particles

MOFs are emerging nanoporous crystals with attractive features, including large surface area, highly regular and tunable pore structure, and structural flexibility inherent to specific types of MOFs (Furukawa H. et al., 2013; Kitagawa S. et al., 2004). In contrast to most conventional adsorbents, such as carbon-based materials and zeolites, which are rigid and typically yield type I isotherms, the structural flexibility of such MOFs is particularly intriguing because their crystal structures transform in response to external stimuli, leading to peculiar adsorption behaviors (Horike S. et al., 2009). Because the peculiar adsorption behaviors are particle size- and shape-dependent (Ehrling S. et al., 2021), controlling the size and shape of MOF particles is an important technology for the practical use of MOFs, and if the mixing matters in the synthetic processes of MOFs, the microreactor is believed to contribute to the development of the technology.

As a model MOF system, we focused on the zeolitic imidazolate framework-8 (ZIF-8), which comprises zinc ions and 2-methylimidazole (2-MIM) linkers (Park K.S. et al., 2006). Although solvothermal syntheses are popular, we selected an environmentally friendly aqueous synthesis process. In the experiment, we mixed aqueous solutions of $Zn(NO_3)_2$ and 2-MIM in a central-collision-type microreactor (**Fig. 1(A)**) (Watanabe S. et al., 2017b). The mixed solution turned turbid within 1 min after being collected from the outlet in a vial. The mixture was allowed to stand for 1 h. **Fig. 13** shows the SEM image and XRD patterns of the resultant particles synthesized at room temperature.

The average diameter of the resultant particles in **Fig. 13(A)** is 434 ± 94 nm with chamfered cubic (CC) shapes composed of square and hexagonal faces. The measured XRD pattern (denoted as "434 nm, CC") agrees fairly well with the simulated pattern for ZIF-8 (Moggach S.A. et al., 2009), demonstrating the successful formation of ZIF-8 particles. The combinations of the concentration of Zn ions, concentration ratio ([2-MIM]/[Zn^{2+}]), and reaction temperature varied the particle size from 51 nm to 1.8 μm and the shape from cubes to CC to rhombic dodecahedron (RD). All of those resultant particles were ZIF-8, as confirmed by the agreement of the XRD patterns with the simulated pattern (**Fig. 13(B)**). The results indicate that the concentration conditions determine the particle size, whereas the reaction temperature defines the particle shape.

The microreactor produced ZIF-8 particles with a sharper size distribution than those synthesized using the batch-type reactor, although the total synthetic period was 1 h, which was much longer than the mixing time. This result is because instantaneous nucleation occurred immediately after quick and homogeneous mixing in the microreactor, which enabled uniform particle growth after collection in a vial. Furthermore, the results also indicate that the reaction conditions in the microreactor govern nucleation, and the temperature in the vial after mixing controls the growth process. Therefore, we developed a concept of setting different temperatures in the microreactor and vial to further control the ZIF-8 particle size and shape. In the experiment, we set the temperature of the microreactor to 5 °C, rapidly increased the temperature of the mixed solution to 80 °C using the central-collision-type microreactor as a microchannel heat exchanger, and collected the heated solution in a vial immersed in a water bath maintained at 80 °C (**Fig. 14(A)**). The size and shape of the resultant particles were 410 ± 86 nm and rhombic dodecahedron, respectively, as shown in **Fig. 14(B)**. The resultant size was almost identical to that synthesized at a temperature of 5 °C throughout the entire synthetic process, but the resultant shape was different (cube at 5 °C). This result demonstrates that the mixing process in the microreactor governs the particle size, whereas the aging process in the vial determines the particle shape. It also exhibits the possibility of separate control of the ZIF-8 particle size and shape by setting different temperatures during nucleation at the microreactor and growth in the

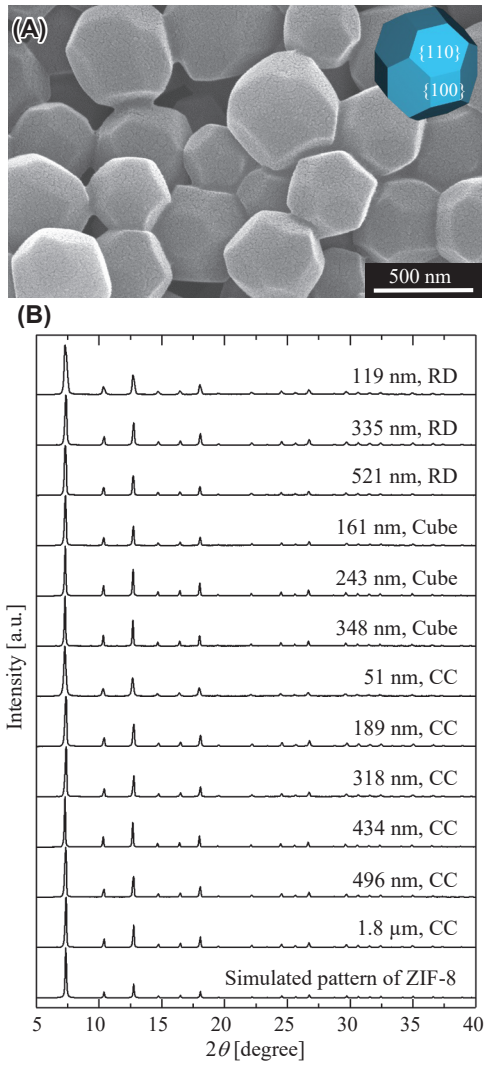

Fig. 13 Synthesis results for ZIF-8 particles using the microreactor. **(A)** Typical SEM image of the resultant particles and **(B)** measured XRD patterns of ZIF-8 particles of various sizes and shapes. Adapted with permission from Ref. (Watanabe S. et al., 2017b). Copyright: (2017) Elsevier B.V.

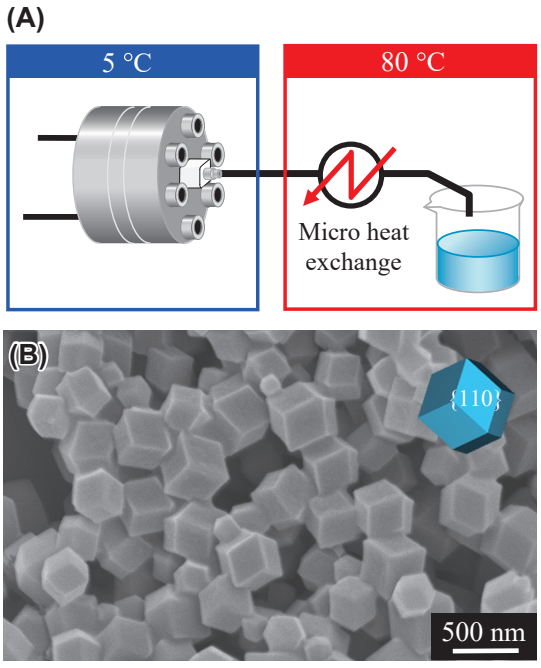

Fig. 14 **(A)** Schematic illustration of the experimental setup with different temperatures set in the microreactor and vial using a micro-heat exchanger. **(B)** SEM image of the ZIF-8 particles prepared at a temperature of 5 °C in the microreactor, followed by rapid temperature increase up to 80 °C. Reprinted with permission from Ref. (Watanabe S. et al., 2017b). Copyright: (2017) Elsevier B.V.

vial. We emphasize that the rapid temperature change was realized by taking full advantage of the characteristics of the flow microreactor process, which would not be possible with batch reactors.

Further functionalization of ZIF-8 particles is possible by encapsulating them in another nanoporous material to form core–shell structures. As a shell material, we used ZIF-67, which is a structural analog of ZIF-8 with cobalt ions instead of zinc ions (Banerjee R. et al., 2008). Because of the crystal structure similarity, seamless growth of ZIF-67 shells was expected on core ZIF-8 particles. In the experiment, we mixed a methanol solution of $Co(NO_3)_2$ with a premixed methanol suspension of ZIF-8 particles and 2-MIM in the central-collision-type microreactor, collected the reaction suspension in a vial, and allowed it to stand for 1 h (Fujiwara A. et al., 2021). We used methanol as the solvent instead of water because ZIF-8 crystals partly dissolve in water. Typical synthetic results are displayed in **Fig. 15**. Polyhedral particles were obtained (**Fig. 15(A)**), and the STEM-EDX mapping image showed that Zn domains were covered with Co domains in single particles (**Fig. 15(B)**), demonstrating the successful synthesis of ZIF-8@ZIF-67 core–shell particles. The ZIF-67 shell thickness increased from 32 nm to 66 nm with decreasing the core particle concentration (**Figs. 15(C)–(E)**). This was possibly because an increased number of Co ions was used for the formation of shells per core particle. Furthermore, the shell thickness was found to be uniform because the particle size distributions simply shifted to larger sizes with coefficient of variance (CV) values remaining almost unchanged after the shell formation reaction (**Figs. 15(F)–(H)**), whereas the size distribution of the ZIF-8@ZIF-67 particles synthesized using the batch reactor was much wider. In addition, no single-component ZIF-67 particles were observed during microreactor synthesis. These results were attributable to the uniform reaction field provided by the microreactor, which facilitated the uniform distribution of Co ions around the core ZIF-8 particles during the shell formation reaction, thereby demonstrating that rapid and homogeneous mixing was critical to realize uniform shell thickness.

By using ZIF-67 particles as the core material and

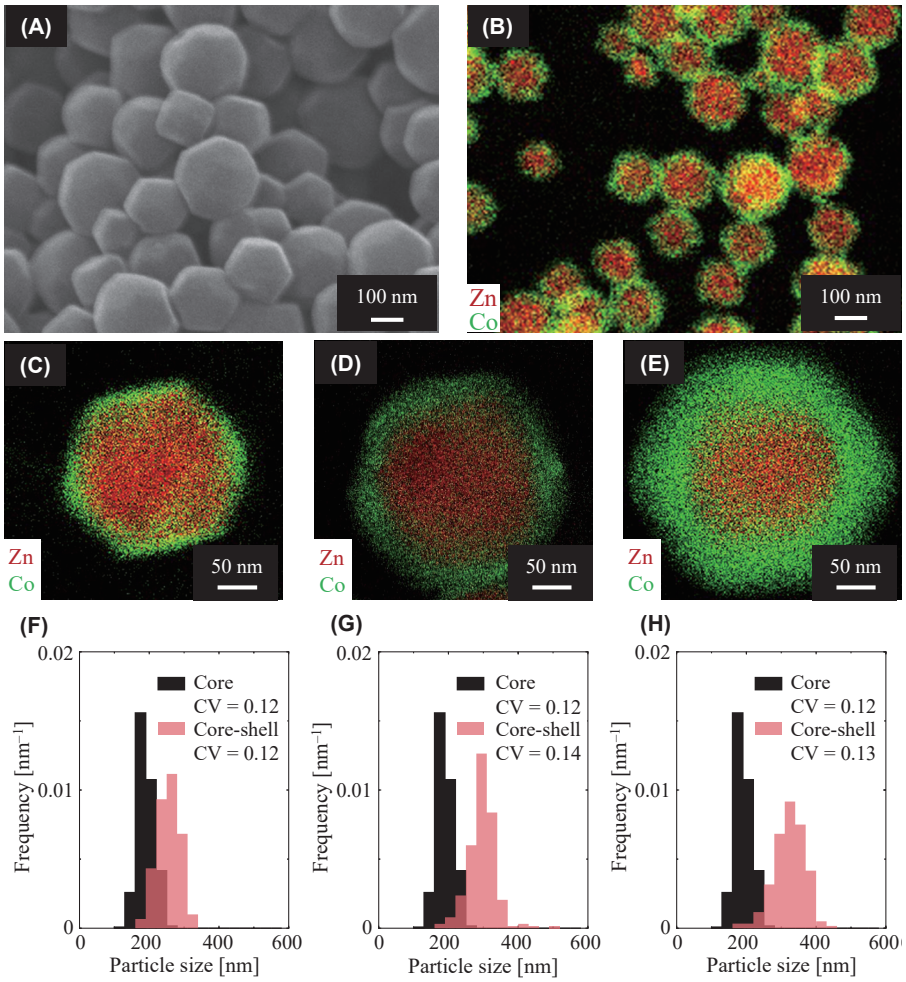

Fig. 15 **(A)** SEM and **(B)** STEM-EDX mapping images of ZIF-8@ZIF-67 particles. **(C–E)** SETM-EDX mapping images and **(F–H)** corresponding size distributions of the resultant particles synthesized at various concentrations. Adapted with permission from Ref. (Fujiwara A. et al., 2021). Copyright: (2021) American Chemical Society.

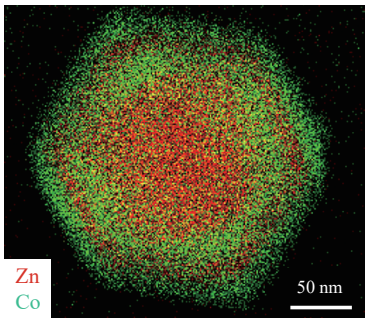

Fig. 16 STEM-EDX mapping image of a ZIF-8@ZIF-67@ZIF-8@ZIF-67 multilayered particle. Adapted with permission from Ref. (Fujiwara A. et al., 2021). Copyright: (2021) American Chemical Society.

$Zn(NO_3)_2$ as the shell source, a swapped structure of ZIF-67@ZIF-8 core–shell particles can also be synthesized using the same synthetic procedure. Furthermore, by repeating the formation processes of the ZIF-67 and ZIF-8 shells, more complex ZIF-8@ZIF-67@ZIF-8@ZIF-67 multilayered structures can be obtained (**Fig. 16**). Zn and Co domains alternately formed shells of similar thickness in a single particle. Because shell formation is initiated by a universal heterogeneous reaction on the core surface, our technique can be extended to the synthesis of "mixed" MOFs with three or more components, aiming at further functionalization of the resultant composites.

6. Conclusions

In this review, we introduced the synthesis of functional NPs, including single-component Ni, Pt–Co alloys, gold and silver nanoshells, patchy particles, CSCs, and nanoporous MOF particles and their core–shell derivatives, using a central-collision-type microreactor. In the case of quick reactions, where the mixing process is often a rate-controlling step, the use of a microreactor with excellent mixing performance is demonstrated to be effective in synthesizing uniform particles in size, shape, and shell thickness. The microreactor is mobile and enables the on-site and on-demand syntheses of functional NPs. Another advantage of the microreactor is its high reproducibility in contrast to conventional batch syntheses, which sometimes suffer from poor reproducibility. A key factor is the relative rate of mixing to the reaction. By adjusting the mixing intensity by the flow rate and reactor geometry according to the reaction rates, synthetic processes can be further optimized in terms of throughput and energy consumption. We hope that this review conveys the advantages of the microreactor and accelerates its industrial use for the precise synthesis of functional NPs.

Nomenclature

CC	Chamfered cube
CSC	Core–shell cluster
CTAB	Cetyltrimethylammonium bromide
CV	Coefficient of variance
EDX	Energy-dispersive X-ray
fcc	Face-centered cubic
MOF	Metal–organic framework
NP	Nanoparticles
PVP	Polyvinylpyrrolidone
RD	Rhombic dodecahedron
STEM	Scanning transmission electron microscopy
TEM	Transmission electron microscopy
VD	Villermaux–Dushman
XPS	X-ray photoelectron spectroscopy
XRD	Powder X-ray diffraction
ZIF	Zeolitic imidazolate framework
t_m	Mixing time (s)

References

Abhinav K.V., Rao R.V.K., Karthik P.S., Singh S.P., Copper conductive inks: synthesis and utilization in flexible electronics, RSC Advances, 5 (2015) 63985–64030. https://doi.org/10.1039/c5ra08205f

Banerjee R., Phan A., Wang B., Knobler C., Furukawa H., O'Keeffe M., Yaghi O.M., High-throughput synthesis of zeolitic imidazolate frameworks and application to CO_2 capture, Science, 319 (2008) 939–943. https://doi.org/10.1126/science.1152516

Chen D.-H., Hsieh C.-H., Synthesis of nickel nanoparticles in aqueous cationic surfactant solutions, Journal of Materials Chemistry, 12 (2002) 2412–2415. https://doi.org/10.1039/b200603k

Chen D.-H., Wu S.-H., Synthesis of nickel nanoparticles in water-in-oil microemulsions, Chemistry of Materials, 12 (2000) 1354–1360. https://doi.org/10.1021/cm991167y

Chen Z., Pei Z., Zhao X., Zhang J., Wei J., Hao N., Acoustic microreactors for chemical engineering, Chemical Engineering Journal, 433 (2022) 133258. https://doi.org/10.1016/j.cej.2021.133258

Commenge J.-M., Falk L., Villermaux–Dushman protocol for experimental characterization of micromixers, Chemical Engineering and Processing: Process Intensification, 50 (2011) 979–990. https://doi.org/10.1016/j.cep.2011.06.006

Couto G.G., Klein J.J., Schreiner W.H., Mosca D.H., de Oliveira A.J., Zarbin A.J., Nickel nanoparticles obtained by a modified polyol process: synthesis, characterization, and magnetic properties, Journal of Colloid and Interface Science, 311 (2007) 461–468. https://doi.org/10.1016/j.jcis.2007.03.045

Domínguez-Crespo M.A., Ramírez-Meneses E., Montiel-Palma V., Torres Huerta A.M., Dorantes Rosales H., Synthesis and electrochemical characterization of stabilized nickel nanoparticles, International Journal of Hydrogen Energy, 34 (2009) 1664–1676. https://doi.org/10.1016/j.ijhydene.2008.12.012

Duraiswamy S., Khan S.A., Plasmonic nanoshell synthesis in microfluidic composite foams, Nano Letters, 10 (2010) 3757–3763. https://doi.org/10.1021/nl102478q

Ehrfeld W., Golbig K., Hessel V., Löwe H., Richter T., Characterization of mixing in micromixers by a test reaction: single mixing units and mixer arrays, Industrial & Engineering Chemistry Research, 38 (1999) 1075–1082. https://doi.org/10.1021/ie980128d

Ehrling S., Miura H., Senkovska I., Kaskel S., From macro- to nanoscale: finite size effects on metal–organic framework switchability, Trends in Chemistry, 3 (2021) 291–304. https://doi.org/10.1016/j.trechm.2020.12.012

Eluri R., Paul B., Synthesis of nickel nanoparticles by hydrazine reduction: mechanistic study and continuous flow synthesis, Journal of Nanoparticle Research, 14 (2012) 800. https://doi.org/10.1007/s11051-012-0800-1

Ely T.O., Amiens C., Chaudret B., Snoeck E., Verelst M., Respaud M., Broto J.-M., Synthesis of nickel nanoparticles. influence of aggregation induced by modification of poly(vinylpyrrolidone) chain length on their magnetic properties, Chemistry of Materials, 11 (1999) 526–529. https://doi.org/10.1021/cm980675p

Fiévet F., Ammar-Merah S., Brayner R., Chau F., Giraud M., Mammeri F.,

Peron J., Piquemal J.Y., Sicard L., Viau G., The polyol process: a unique method for easy access to metal nanoparticles with tailored sizes, shapes and compositions, Chemical Society Reviews, 47 (2018) 5187–5233. https://doi.org/10.1039/c7cs00777a

Fournier M.C., Falk L., Villermaux J., A new parallel competing reaction system for assessing micromixing efficiency—Determination of micromixing time by a simple mixing model, Chemical Engineering Science, 51 (1996) 5187–5192. https://doi.org/10.1016/S0009-2509(96)00340-5

Fujiwara A., Watanabe S., Miyahara M.T., Flow microreactor synthesis of zeolitic imidazolate framework (ZIF)@ZIF core-shell metal-organic framework particles and their adsorption properties, Langmuir, 37 (2021) 3858–3867. https://doi.org/10.1021/acs.langmuir.0c03378

Furukawa H., Cordova K.E., O'Keeffe M., Yaghi O.M., The chemistry and applications of metal-organic frameworks, Science, 341 (2013) 1230444. https://doi.org/10.1126/science.1230444

Gilbert E.C., Evans W.H., Complex formation between nickel ion and hydrazine in solution, Journal of the American Ceramic Society, 73 (1951) 3516–3518. https://doi.org/10.1021/ja01151a518

Gioria E., Wisniewski F., Gutierrez L., Microreactors for the continuous and green synthesis of palladium nanoparticles: enhancement of the catalytic properties, Journal of Environmental Chemical Engineering, 7 (2019) 103136. https://doi.org/10.1016/j.jece.2019.103136

Gutierrez L., Gomez L., Irusta S., Arruebo M., Santamaria J., Comparative study of the synthesis of silica nanoparticles in micromixer–microreactor and batch reactor systems, Chemical Engineering Journal, 171 (2011) 674–683. https://doi.org/10.1016/j.cej.2011.05.019

Han J.H., Kim D., Kim J., Kim G., Fischer P., Jeong H.H., Plasmonic nanostructure engineering with shadow growth, Advanced Materials, (2022) e2107917. https://doi.org/10.1002/adma.202107917

Hashiguchi Y., Watanabe F., Honma T., Nakamura I., Poly S.S., Kawaguchi T., Tsuji T., Murayama H., Tokunaga M., Fujitani T., Continuous-flow synthesis of Pd@Pt core-shell nanoparticles, Colloids and Surfaces A: Physicochemical and Engineering Aspects, 620 (2021) 126607. https://doi.org/10.1016/j.colsurfa.2021.126607

Horike S., Shimomura S., Kitagawa S., Soft porous crystals, Nature Chemistry, 1 (2009) 695–704. https://doi.org/10.1038/nchem.444

Hou J., Yang M., Ke C., Wei G., Priest C., Qiao Z., Wu G., Zhang J., Platinum-group-metal catalysts for proton exchange membrane fuel cells: from catalyst design to electrode structure optimization, EnergyChem, 2 (2020) 100023. https://doi.org/10.1016/j.enchem.2019.100023

Jiang B., Li C., Imura M., Tang J., Yamauchi Y., Multimetallic mesoporous spheres through surfactant-directed synthesis, Advanced Science, 2 (2015) 1500112. https://doi.org/10.1002/advs.201500112

Jiang Z., Xie J., Jiang D., Wei X., Chen M., Modifiers-assisted formation of nickel nanoparticles and their catalytic application to *p*-nitrophenol reduction, CrystEngComm, 15 (2013) 560–569. https://doi.org/10.1039/c2ce26398j

Kitagawa S., Kitaura R., Noro S., Functional porous coordination polymers, Angewandte Chemie International Edition, 43 (2004) 2334–2375. https://doi.org/10.1002/anie.200300610

Li Y.D., Li L.Q., Liao H.W., Wang H.R., Preparation of pure nickel, cobalt, Nickel-cobalt and nickel-copper alloys by hydrothermal reduction, Journal of Materials Chemistry, 9 (1999) 2675–2677. https://doi.org/10.1039/A904686K

Lin X.Z., Terepka A.D., Yang H., Synthesis of silver nanoparticles in a continuous flow tubular microreactor, Nano Letters, 4 (2004) 2227–2232. https://doi.org/10.1021/nl0485859

Luty-Błocho M., Wojnicki M., Pacławski K., Fitzner K., The synthesis of platinum nanoparticles and their deposition on the active carbon fibers in one microreactor cycle, Chemical Engineering Journal, 226 (2013) 46–51. https://doi.org/10.1016/j.cej.2013.04.008

Mae K., Advanced chemical processing using microspace, Chemical Engineering Science, 62 (2007) 4842–4851. https://doi.org/10.1016/j.ces.2007.01.012

Maw S.S., Watanabe S., Miyahara M.T., Flow synthesis of silver nanoshells using a microreactor, Chemical Engineering Journal, 374 (2019) 674–683. https://doi.org/10.1016/j.cej.2019.05.210

Meincke T., Bao H., Pflug L., Stingl M., Klupp Taylor R.N., Heterogeneous nucleation and surface conformal growth of silver nanocoatings on colloidal silica in a continuous flow static T-mixer, Chemical Engineering Journal, 308 (2017) 89–100. https://doi.org/10.1016/j.cej.2016.09.048

Moggach S.A., Bennett T.D., Cheetham A.K., The effect of pressure on ZIF-8: increasing pore size with pressure and the formation of a high-pressure phase at 1.47 GPa, Angewandte Chemie International Edition, 48 (2009) 7087–7089. https://doi.org/10.1002/anie.200902643

Mühlig S., Cunningham A., Scheeler S., Pacholski C., Bürgi T., Rockstuhl C., Lederer F., Self-assembled plasmonic core-shell clusters with an isotropic magnetic dipole response in the visible range, ACS Nano, 5 (2011) 6586–6592. https://doi.org/10.1021/nn201969h

Nagasawa H., Aoki N., Mae K., Design of a new micromixer for instant mixing based on the collision of micro segments, Chemical Engineering and Technology, 28 (2005) 324–330. https://doi.org/10.1002/ceat.200407118

Oldenburg S.J., Averitt R.D., Westcott S.L., Halas N.J., Nanoengineering of optical resonances, Chemical Physics Letters, 288 (1998) 243–247. https://doi.org/10.1016/S0009-2614(98)00277-2

Park J.W., Chae E.H., Kim S.H., Lee J.H., Kim J.W., Yoon S.M., Choi J.-Y., Preparation of fine Ni powders from nickel hydrazine complex, Materials Chemistry and Physics, 97 (2006) 371–378. https://doi.org/10.1016/j.matchemphys.2005.08.028

Park K.S., Ni Z., Cote A.P., Choi J.Y., Huang R., Uribe-Romo F.J., Chae H.K., O'Keeffe M., Yaghi O.M., Exceptional chemical and thermal stability of zeolitic imidazolate frameworks, Proceedings of the National Academy of Sciences, 103 (2006) 10186–10191. https://doi.org/10.1073/pnas.0602439103

Rasch M.R., Sokolov K.V., Korgel B.A., Limitations on the optical tunability of small diameter gold nanoshells, Langmuir, 25 (2009) 11777–11785. https://doi.org/10.1021/la901249j

Saha K., Agasti S.S., Kim C., Li X., Rotello V.M., Gold nanoparticles in chemical and biological sensing, Chemical Reviews, 112 (2012) 2739–2779. https://doi.org/10.1021/cr2001178

Sharada S., Suryawanshi P.L., Kumar P R., Gumfekar S.P., Narsaiah T.B., Sonawane S.H., Synthesis of palladium nanoparticles using continuous flow microreactor, Colloids and Surfaces A: Physicochemical and Engineering Aspects, 498 (2016) 297–304. https://doi.org/10.1016/j.colsurfa.2016.03.068

Suryawanshi P.L., Gumfekar S.P., Kumar P.R., Kale B.B., Sonawane S.H., Synthesis of ultra-small platinum nanoparticles in a continuous flow microreactor, Colloid and Interface Science Communications, 13 (2016) 6–9. https://doi.org/10.1016/j.colcom.2016.05.001

Völkl A., Klupp Taylor R.N., Investigation and mitigation of reagent ageing during the continuous flow synthesis of patchy particles, Chemical Engineering Research and Design, 181 (2022) 133–143. https://doi.org/10.1016/j.cherd.2022.03.016

Wagner J., Kirner T., Mayer G., Albert J., Köhler J.M., Generation of metal nanoparticles in a microchannel reactor, Chemical Engineering Journal, 101 (2004) 251–260. https://doi.org/10.1016/j.cej.2003.11.021

Wagner J., Köhler J.M., Continuous synthesis of gold nanoparticles in a microreactor, Nano Letters, 5 (2005) 685–691. https://doi.org/10.1021/nl050097t

Wang D., Li Y., Bimetallic nanocrystals: liquid-phase synthesis and catalytic applications, Advanced Materials, 23 (2011) 1044–1060. https://doi.org/10.1002/adma.201003695

Watanabe S., Asahi Y., Omura H., Mae K., Miyahara M.T., Flow microreactor synthesis of gold nanoshells and patchy particles, Advanced Powder Technology, 27 (2016) 2335–2341. https://doi.org/10.1016/j.apt.2016.08.013

Watanabe S., Hiratsuka T., Asahi Y., Tanaka A., Mae K., Miyahara M.T., Flow synthetic process of SiO_2@Au core-shell nanoparticles by using microreactor, Journal of the Society of Powder Technology, Japan, 50 (2013) 478–484. https://doi.org/10.4164/sptj.50.478

Watanabe S., Hiratsuka T., Asahi Y., Tanaka A., Mae K., Miyahara M.T., Flow synthesis of plasmonic gold nanoshells via a microreactor, Particle & Particle Systems Characterization, 32 (2015) 234–242.

https://doi.org/10.1002/ppsc.201400126
Watanabe S., Koshiyama T., Watanabe T., Miyahara M.T., Room-temperature synthesis of Ni and Pt-Co alloy nanoparticles using a microreactor, Frontiers in Chemical Engineering, 3 (2021) 780384. https://doi.org/10.3389/fceng.2021.780384
Watanabe S., Ohsaki S., Fukuta A., Hanafusa T., Takada K., Tanaka H., Maki T., Mae K., Miyahara M.T., Characterization of mixing performance in a microreactor and its application to the synthesis of porous coordination polymer particles, Advanced Powder Technology, 28 (2017a) 3104–3110. https://doi.org/10.1016/j.apt.2017.09.005
Watanabe S., Ohsaki S., Hanafusa T., Takada K., Tanaka H., Mae K., Miyahara M.T., Synthesis of zeolitic imidazolate framework-8 particles of controlled sizes, shapes, and gate adsorption characteristics using a central collision-type microreactor, Chemical Engineering Journal, 313 (2017b) 724–733. https://doi.org/10.1016/j.cej.2016.12.118
Wolfbeis O.S., An overview of nanoparticles commonly used in fluorescent bioimaging, Chemical Society Reviews, 44 (2015) 4743–4768. https://doi.org/10.1039/c4cs00392f
Wu K.-J., De Varine Bohan G.M., Torrente-Murciano L., Synthesis of narrow sized silver nanoparticles in the absence of capping ligands in helical microreactors, Reaction Chemistry & Engineering, 2 (2017) 116–128. https://doi.org/10.1039/c6re00202a
Wu S.-H., Chen D.-H., Synthesis and characterization of nickel nanoparticles by hydrazine reduction in ethylene glycol, Journal of Colloid and Interface Science, 259 (2003) 282–286. https://doi.org/10.1016/s0021-9797(02)00135-2
Wu S.-H., Chen D.-H., Synthesis and stabilization of Ni nanoparticles in a pure aqueous CTAB solution, Chemistry Letters, 33 (2004) 406–407. https://doi.org/10.1246/cl.2004.406
Wu X., Xing W., Zhang L., Zhuo S., Zhou J., Wang G., Qiao S., Nickel nanoparticles prepared by hydrazine hydrate reduction and their application in supercapacitor, Powder Technology, 224 (2012) 162–167. https://doi.org/10.1016/j.powtec.2012.02.048
Xia Y., Xiong Y., Lim B., Skrabalak S.E., Shape-controlled synthesis of metal nanocrystals: simple chemistry meets complex physics?, Angewandte Chemie International Edition, 48 (2009) 60–103. https://doi.org/10.1002/anie.200802248
Xu L., Srinivasakannan C., Peng J., Zhang D., Chen G., Synthesis of nickel nanoparticles by aqueous reduction in continuous flow microreactor, Chemical Engineering and Processing: Process Intensification, 93 (2015) 44–49. https://doi.org/10.1016/j.cep.2015.04.010
Yang W., Liang H., Ma S., Wang D., Huang J., Gold nanoparticle based photothermal therapy: development and application for effective cancer treatment, Sustainable Materials and Technologies, 22 (2019) e00109. https://doi.org/10.1016/j.susmat.2019.e00109
Yoshida J., Takahashi Y., Nagaki A., Flash chemistry: flow chemistry that cannot be done in batch, Chemical Communications, 49 (2013) 9896–9904. https://doi.org/10.1039/c3cc44709j

Authors' Short Biographies

Dr. Satoshi Watanabe is an Associate Professor of Department of Chemical Engineering at Kyoto University. He earned his B.S., M.S., and Ph.D. (Chemical Engineering) from Kyoto University. He has worked for Kyoto University as an Assistant Professor, Junior Associate Professor, and Associate Professor. His research is in the field of colloid science and engineering, especially focusing on material design and technologies to bridge functions and structures from micro- to macroscale.

Prof. Minoru T. Miyahara was a Professor of Department of Chemical Engineering at Kyoto University. He earned his Ph.D. from Kyoto University. He had held key senior positions in academic societies in areas of powder technology, adsorption science and technology, and chemical engineering. He had devoted all his efforts to research and education. He unfortunately passed away in August 2022.